

Mechanical Properties and Thermodynamic Parameters of Sr_2RuO_4 and $\text{Sr}_2\text{RuO}_2\text{F}_2$ Compounds under Pressure and Temperature Effects: Voigt–Reuss–Hill Approximations and Debye Model

Meryem Ziati* and Hamid Ez-Zahraouy

Laboratory of Condensed Matter and Interdisciplinary Sciences, Department of Physics, Faculty of Sciences, Mohammed V University in Rabat, Morocco

ABSTRACT

We present a first-principles study of the elastic and thermodynamic properties of the $\text{Sr}_2\text{RuO}_4-x\text{F}_x$ alloy ($x = 0, 2$). Computations are carried out using the WIEN2K code based on a non-relativistic full-potential linearized augmented plane wave (FP-LAPW) method within the density functional theory (DFT). The Voigt–Reuss–Hill approximation method is applied to analyze the elastic constants, Poisson ratio, bulk, shear, and Young modulus at zero pressure and temperature using ELASTIC 1.0 software. The Sr_2RuO_4 and $\text{Sr}_2\text{RuO}_2\text{F}_2$ tetragonal phases are mechanically stable because the elastic constants satisfy Born's mechanical stability condition. In addition, we performed a quasi-harmonic Debye model calculation using the GIBBS2 package to predict the thermodynamic properties and their temperature and pressure dependencies. Thermodynamic parameters such as the Gibbs free energy, heat capacity, Grüneisen parameter, and Debye temperature are successfully obtained and discussed.

*Corresponding author

Meryem Ziati, Laboratory of Condensed Matter and Interdisciplinary Sciences, Department of Physics, Faculty of Sciences, Mohammed V University in Rabat, Morocco. Email: meryem.ziati.um5@gmail.com

Received: November 26, 2021; **Accepted:** December 09, 2021; **Published:** December 15, 2021

Keywords: DFT, Thermodynamic Properties, Elastic properties, Debye model, GIBBS2.

Introduction

The family of ruthenium oxides, ruthenates, emerged a few years after the discovery of the copper oxides and cuprates at the IBM laboratory in Zurich [1]. The structure of Sr_2RuO_4 is quite similar to that of the first superconducting cuprate La_2CuO_4 discovered in 1986, i.e., a perovskite structure [2]. Simply, the copper atoms are replaced by ruthenium atoms and lanthanum atoms by strontium elements. The Sr_2RuO_4 unit cell ($I4/mmm$) is a stoichiometric compound and chemically possesses significant stability [3].

Transition-metal oxides have attracted considerable interest due to their rich physical properties such as metal–insulator transition, exotic superconductivity, spin–charge–orbital ordering, etc. The discovery of superconductivity in Sr_2RuO_4 at about 1.5 K in 1994 [4]. Until today, most high-temperature superconductors (HTCS) have possessed CuO_2 planes as their basic structural units. Investigations reveal that the high hybridization between the Cu $3d_{x^2-y^2}$ and O $2p$ orbitals, the intense electron–electron correlation at the Cu site, and the charge transfer character around the Fermi level, have an important effect on the superconductivity in these materials [5]. Sr_2RuO_4 is attractive because some other compounds isostructural to the cuprate superconductors, such as La_2NiO_4 and Sr_2RhO_4 , are not superconductors. Hence the discovery of Sr_2RuO_4 provides an opportunity to study the overall characteristics of the HTCS.

Theoretically, the magnetic excitations in the Sr_2RuO_4 compound are extensively studied by M. Braden et al. through inelastic neutron scattering [6]. The in-plane and out-of-plane optical spectra, magneto-resistance and resistivity at different temperatures, X-ray fluorescence emission, and the improvement of superconductivity by doping are studied to encompass all features of this crystal [7–11]. Furthermore, several efforts are carried out by Hashimoto et al. to prove that strontium ruthenate is believed to be a spin-triplet superconductor at low temperatures [12]. The preliminary computations reported by T. Oguchi et al., based on bare DFT suggest that the Fermi surface of Sr_2RuO_4 comprises three dissimilar sheets: two electron-like sheets located around the Γ -point and a hole-like one centered at the X-point [13].

This research paper aims to give a detailed description of the elastic and thermodynamic properties of the Sr_2RuO_4 and $\text{Sr}_2\text{RuO}_2\text{F}_2$ alloys under hydrostatic pressure and temperature effect, using the FP-LAPW method within density functional theory (DFT) as implemented in the WIEN2K software.

Computational Details

Elastic and thermodynamic properties of the Sr_2RuO_4 and $\text{Sr}_2\text{RuO}_2\text{F}_2$ compounds are probed via first-principles full-potential linearized augmented-plane-wave (FP-LAPW) method within the DFT scheme as implemented in WIEN2K ab initio simulation program [14]. We applied the generalized gradient approximation presented by Perdew–Burke–Ernzerhof (GGA-PBE) to describe

the exchange-correlation effects and to evaluate the ground state parameters [15]. Tran Balaha modified Becke-Johnson exchange potential (TB-mBJ) is implemented to overcome deficiencies in the electronic properties and bandgap calculations [16]. The static computations are performed using a dense mesh ($10 \times 10 \times 10$) k-points grid in reciprocal space (in the first Brillouin zone). The self-consistent criterion is selected with an accuracy of 10^{-6} Ry, while the iterations are halted when the force convergence threshold is approximately 10^{-4} eV/Å. The product of the maximum modulus of reciprocal vector (K_{max}) and the smallest of all atomic sphere radii (R_{min}) is 8 ($K_{\text{max}} \times R_{\text{min}} = 8$). The cut-off energy which defines the core-valence state separation is chosen to be -6.0 Ry. The other input feedings of the WIEN2K software are chosen as $l_{\text{max}} = 10$ and $G_{\text{max}} = 16.1$. l_{max} exhibits the maximum value of the angular momentum vector and G_{max} presents the Fourier-expanded charge density.

Electronic Properties

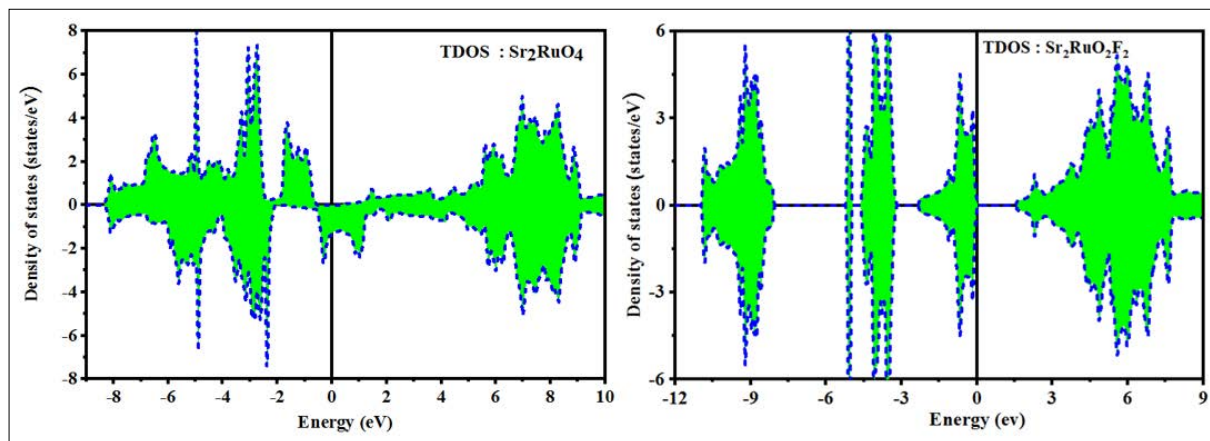


Figure 1: Spin-polarized total densities of states for Sr_2RuO_4 and $\text{Sr}_2\text{RuO}_2\text{F}_2$ compounds.

The superconductor Sr_2RuO_4 (no.139) consists of alternative monolayers piled up along the c-axis and suggests a metallic ground state [17] (see Fig. 1). The fractional atomic coordinates are defined by Sr: $4e(0,0,Z_{\text{Sr}})$; Ru: $2a(0,0,0)$; $\text{O}_{(1)}$: $4e(0,0,Z_{\text{O}})$ and $\text{O}_{(2)}$ / F: $4c(0,0.5,0)$ ($Z_{\text{Sr}} = 0.3527$; $Z_{\text{O}} = 0.1607$). The optimized lattice parameters are listed in Table 1. The $\text{Sr}_2\text{RuO}_{4-x}\text{F}_x$ quaternary alloy ($x = 2$) is formed by substituting the oxygen, which defines the shortest Ru – $\text{O}_{(2)}$ bonds in the *ab* plane with fluorine atoms. The suggested substitution relocated the bands and displaced the electronic states from the Fermi level to lower energy levels creating an electronic bandgap, as presented in Fig. 1. Usually, the intensity and interaction between atoms are widely alerted after the substitution process. The electronic band structures of the Sr_2RuO_4 and $\text{Sr}_2\text{RuO}_2\text{F}_2$ compounds along the high symmetry points of the Brillouin zone using the spin-polarized GGA-PBE + TB-mBJ approximations are depicted in Fig. 2 (a) - (b) and Fig. 3.

Fig. 2 (a) - (b). illustrates that there are three bands lightly intersect the Fermi level, which proves that the minority spin exhibits a metallic behavior. The majority spin presents a semiconducting demeanor, and the total contributions of both minority spin and majority spin states suggest a metallic ground state of the Sr_2RuO_4 compound.

Fig. 3 demonstrates that the valence band maxima (VBM) and the conduction band minima (CBM) for F – doped Sr_2RuO_4 occur at M and Γ points. Hence, the $\text{Sr}_2\text{RuO}_2\text{F}_2$ quaternary alloy exhibits an indirect bandgap of 1.5 eV.

Table 1: Equilibrium lattice constants of Sr_2RuO_4 and $\text{Sr}_2\text{RuO}_2\text{F}_2$ using the GGA-PBE approximation

	Present work			Other works			Experimental		
	a (Å)	a/b	c (Å)	a (Å)	a/b	c (Å)	a (Å)	a/b	c (Å)
Sr_2RuO_4	3.85	1	12.78	3.84 [17]	1	12.78 [17]	3.9 [18]	1	12.7 [18]
$\text{Sr}_2\text{RuO}_2\text{F}_2$	3.98	1	13.40	3.98 [17]	1	13.23 [17]	(-)	(-)	

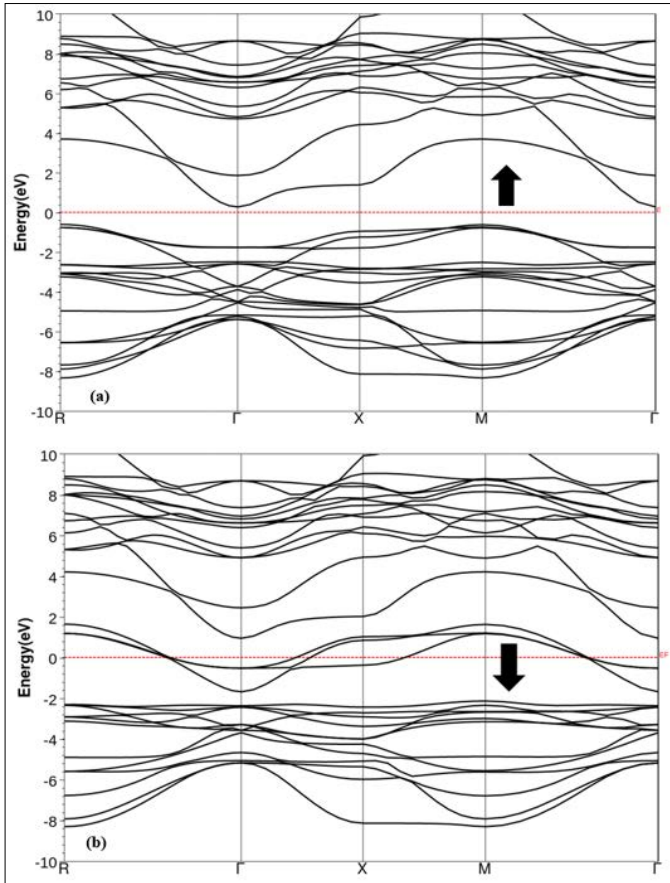


Figure 2 (a) - (b): Spin-polarized band structures of Sr_2RuO_4 [(a) Spin up / (b) Spin down]

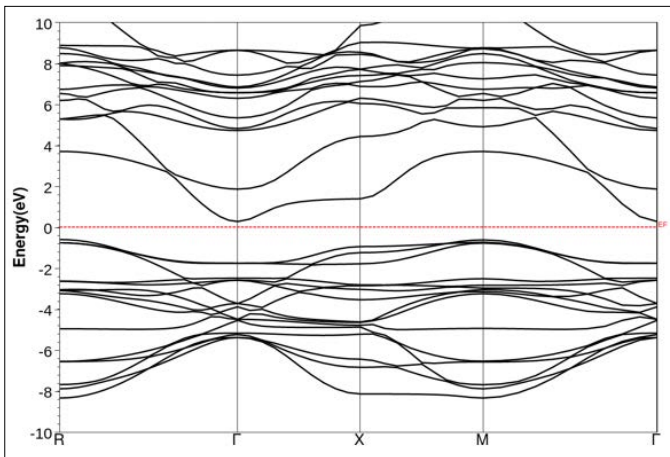


Figure 3: Spin-polarized band structures of $\text{Sr}_2\text{RuO}_2\text{F}_2$ alloy.

Elastic Properties

The elastic property is an important feature of solids. It is closely related to various fundamental physical properties, such as specific heat, melting point, Debye temperature, thermal expansion coefficient, etc. The elastic tensor C_{ij} is derived by performing six finite distortions of the lattice and deriving the elastic constants from the strain-stress relationship [19]. Other elastic properties can be ascertained based on the computed elastic constants C_{ij} , such as bulk modulus (B) and shear modulus (G). Two different theories are employed to assess the elastic moduli [20]: Reuss theory (B_R and G_R) and Voigt theory (B_V and G_V) [21]:

$$B_V = \frac{1}{9} [(C_{11} + C_{22} + C_{33}) + 2(C_{12} + C_{23} + C_{31})] \quad (1)$$

$$G_V = \frac{1}{15} [(C_{11} + C_{22} + C_{33}) - 2(C_{12} + C_{23} + C_{31}) + 3(C_{44} + C_{55} + C_{66})] \quad (2)$$

$$\frac{1}{B_R} = (S_{11} + S_{22} + S_{33}) + 2(S_{12} + S_{23} + S_{31}) \quad (3)$$

$$\frac{1}{G_R} = 4(S_{11} + S_{22} + S_{33}) - 4(S_{12} + S_{23} + S_{31}) + 3(S_{44} + S_{55} + S_{66}) \quad (4)$$

C_{ij} is the inverse matrix of S_{ij} , and they exhibit the elastic stiffness coefficients and the elastic compliance coefficients, respectively. On the other hand, there is a so-called Hill theory, where [21]:

$$B_H = (B_V + B_R)/2 \quad (5)$$

$$G_H = (G_V + G_R)/2 \quad (6)$$

Pugh criterion ensures that when B_H/G_H is less (bigger) than 1.75, the material is considered brittle (ductile) [22]. Furthermore, Young's modulus E and Poisson's ratio ν are obtained using the following formulas [23]:

$$E = 9BG / (3B+G) \quad (7)$$

$$\nu = (3B-2G) / [2(3B+G)] \quad (8)$$

For a tetragonal crystal, nine independent single-crystal elastic constants characterize the capacity of a material to deform under small stresses (C_{11} , C_{12} , C_{13} , C_{22} , C_{23} , C_{33} , C_{44} , C_{55} , and C_{66}). The mechanical stability is confirmed using Born's criteria [24]. Against any homogeneous elastic deformation, the material is considered stable when the following conditions are verified:

$$\left. \begin{aligned} (C_{11} - C_{12}) > 0, (C_{11} + C_{33} - 2C_{13}) > 0 \\ C_{11} > 0, C_{22} > 0, C_{44} > 0, C_{66} > 0 \\ (2C_{11} + C_{33} + 2C_{12} + 4C_{13}) > 0 \end{aligned} \right\} \quad (9)$$

First-principles calculation of stress tensors is presented by Nielsen and Martin following Hooke's law ($\sigma_{ij} = C_{ijkl} \epsilon_{kl}$), where σ_{ij} presents the stress tensor, ϵ_{kl} is the Lagrangian strain tensor, and C_{ijkl} is the elastic constant tensor which is 6×6 matrix (36 elements in general cases) [25, 26]. The generalized Hooke's law for a tetragonal structure may be written as [27]:

$$\begin{pmatrix} \sigma_1 \\ \sigma_2 \\ \sigma_3 \\ \tau_1 \\ \tau_2 \\ \tau_3 \end{pmatrix} = \begin{pmatrix} C_{11} & C_{12} & C_{13} & 0 & 0 & 0 \\ C_{21} & C_{22} & C_{23} & 0 & 0 & 0 \\ C_{31} & C_{32} & C_{33} & 0 & 0 & 0 \\ 0 & 0 & 0 & C_{44} & 0 & 0 \\ 0 & 0 & 0 & 0 & C_{55} & 0 \\ 0 & 0 & 0 & 0 & 0 & C_{66} \end{pmatrix} \begin{pmatrix} \epsilon_1 \\ \epsilon_2 \\ \epsilon_3 \\ \gamma_1 \\ \gamma_2 \\ \gamma_3 \end{pmatrix}$$

Where σ_i and τ_i are normal and shear stress, respectively, while ϵ_i and γ_i are normal and shear strains, respectively. The predicted elastic constants (stiffness) and elastic compliances of tetragonal Sr_2RuO_4 and $\text{Sr}_2\text{RuO}_2\text{F}_2$ are presented as a matrix in Voigt notation at 0K:

• Elastic constant (stiffness) matrix in GPa of Sr_2RuO_4 :

$$C_{ij} = \begin{pmatrix} 477.0 & 310.0 & 173.3 & 0 & 0 & 0 \\ 310.0 & 477.0 & 173.3 & 0 & 0 & 0 \\ 173.3 & 173.3 & 587.6 & 0 & 0 & 0 \\ 0 & 0 & 0 & 75.7 & 0 & 0 \\ 0 & 0 & 0 & 0 & 75.7 & 0 \\ 0 & 0 & 0 & 0 & 0 & 63.9 \end{pmatrix}$$

• **Elastic constant (stiffness) matrix in GPa of $\text{Sr}_2\text{RuO}_2\text{F}_2$:**

$$C_{ij} = \begin{pmatrix} 871.2 & 557.4 & 32.9 & 0 & 0 & 0 \\ 557.4 & 871.2 & 32.9 & 0 & 0 & 0 \\ 32.9 & 32.9 & 695.7 & 0 & 0 & 0 \\ 0 & 0 & 0 & 51.2 & 0 & 0 \\ 0 & 0 & 0 & 0 & 51.2 & 0 \\ 0 & 0 & 0 & 0 & 0 & 9.4 \end{pmatrix}$$

• **Elastic compliance matrix in 1/GPa of Sr_2RuO_4 :**

$$S_{ij} = \begin{pmatrix} 0.00372 & -0.00226 & -0.00043 & 0 & 0 & 0 \\ -0.00226 & 0.00372 & -0.00043 & 0 & 0 & 0 \\ -0.00043 & -0.00043 & 0.00196 & 0 & 0 & 0 \\ 0 & 0 & 0 & 0.01320 & 0 & 0 \\ 0 & 0 & 0 & 0 & 0.01320 & 0 \\ 0 & 0 & 0 & 0 & 0 & 0.01564 \end{pmatrix}$$

• **Elastic compliance matrix in 1/GPa of $\text{Sr}_2\text{RuO}_2\text{F}_2$:**

$$S_{ij} = \begin{pmatrix} 0.00194 & -0.00124 & -0.00003 & 0 & 0 & 0 \\ -0.00124 & 0.00194 & -0.00003 & 0 & 0 & 0 \\ -0.00003 & -0.00003 & 0.00144 & 0 & 0 & 0 \\ 0 & 0 & 0 & 0.01954 & 0 & 0 \\ 0 & 0 & 0 & 0 & 0.01954 & 0 \\ 0 & 0 & 0 & 0 & 0 & 0.10597 \end{pmatrix}$$

The findings suggest that C_{11} , C_{12} , and C_{33} of Sr_2RuO_4 are all smaller than those of $\text{Sr}_2\text{RuO}_2\text{F}_2$, indicating the c-axes of tetragonal Sr_2RuO_4 are easier to be compressed than for the $\text{Sr}_2\text{RuO}_2\text{F}_2$ compound. Furthermore, the values obtained for C_{44} are substantially smaller than those of C_{11} , indicating the resistance of the studied materials to shear deformation along the (100) plane. The reason should be that C_{11} is mainly determined by the stronger and stable polar covalent bond between Ru – 4d and O (1) – 2p / O (2) – 2p electrons that is along the a-axis, while C_{44} is principally determined by the weak hybridization between Ru – 4d / F – p orbitals and the ionicity of Sr – O bonds which are along the c-axis. The lowest value that occurs on C_{66} implies that the shear deformation, corresponding to C_{66} , is the easiest to achieve compared to the other deformations. The wide discrepancies in the elastic constants also indicate that the Sr_2RuO_4 and $\text{Sr}_2\text{RuO}_2\text{F}_2$ materials are mechanically anisotropic. Despite the mismatch of C_{ij} 's between Sr_2RuO_4 and $\text{Sr}_2\text{RuO}_2\text{F}_2$ compounds, the two tetragonal phases are mechanically stable because the elastic constants satisfy the Born's mechanical stability condition. By using the computed elastic constants C_{ij} , the bulk (B) and shear (G) moduli of the crystal structures can be calculated according to the Voigt, Reuss, and Hill approximations, as tabulated in Table 2.

According to Pugh criteria, the BH/GH ratio separates ductile and brittle materials. Brittleness and ductility have a huge influence on the mechanical behavior of a material. For Sr_2RuO_4 , the ratio of BH/GH is 3.38, the discovered finding is consistent, to some extent, with the theoretical investigation previously reported (BH/GH = 2.15) by Xi-Ping Hao et al [28]. For the $\text{Sr}_2\text{RuO}_2\text{F}_2$ compound, the ratio BH/GH calculated using the PBE-GGA+TB-mBJ approach is found to be 4.42. This value is greater than Pugh's critical point, thus $\text{Sr}_2\text{RuO}_2\text{F}_2$ has a ductile feature. Both tetragonal compounds show ductile nature since their BH/GH ratios are > 1.75. The Cauchy relationship which is defined as $C_c = C_{12} - C_{44}$ is an important parameter signifying the ductility or brittleness of a material [26]. The positive value of this parameter ensures the ductility of the material, otherwise, it is brittle when the value is found to be negative. The computed C_c using the PBE-GGA+TB-

mBJ approximation of Sr_2RuO_4 and $\text{Sr}_2\text{RuO}_2\text{F}_2$ is 234.5 GPa and 506.2 GPa, respectively. From these results, we can conclude that the studied materials are ductile, which confirms Pugh's criteria. The bulk modulus is significantly greater than the shear modulus. This result indicates that the shear deformation is easier to occur, and the parameter limiting the stability of Sr_2RuO_4 and $\text{Sr}_2\text{RuO}_2\text{F}_2$ is the shear modulus. Young's modulus and Poisson's ratio are important parameters for selecting materials in engineering design (see Table 2). The Voigt Young's moduli of tetragonal Sr_2RuO_4 and $\text{Sr}_2\text{RuO}_2\text{F}_2$ are predicted to be 276.6 GPa and 385.12 GPa, while the Voigt Poisson's ratios are 0.35 and 0.34, respectively.

The elastic anisotropy Λ is strongly related to the probability of promoting micro-cracks in the solids. For an isotropic crystal, the elastic anisotropy is about 1. With any deviation from the unity, the crystal becomes anisotropic. The simulated compounds Sr_2RuO_4 and $\text{Sr}_2\text{RuO}_2\text{F}_2$ have anisotropic factors of 0.10 and 0.63, respectively. Therefore, they are robust anisotropic crystals.

Thermodynamic Properties

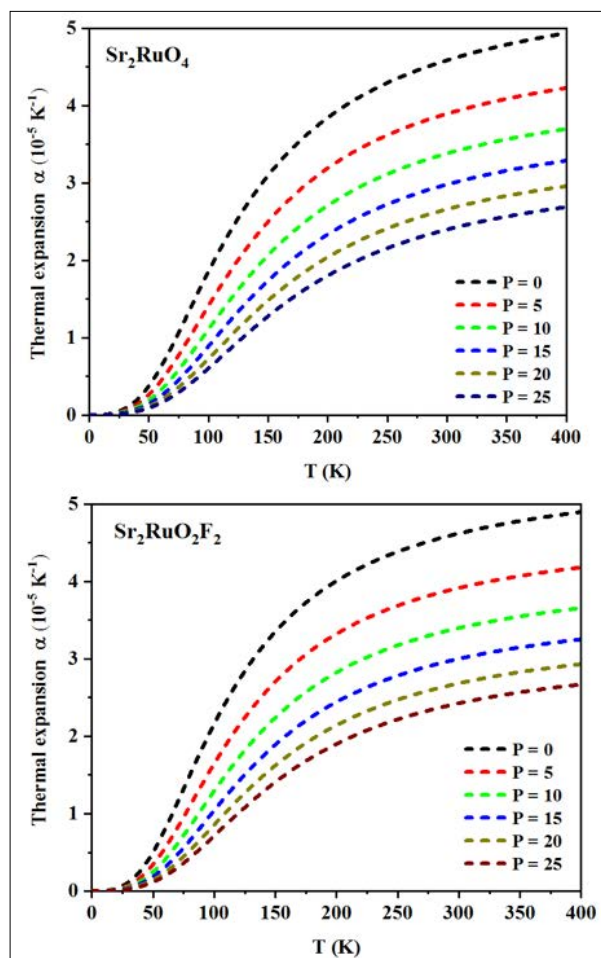


Figure 4: The thermal expansion coefficient as a function temperatures at different pressures

Fig. 4. shows the evolution of the thermal expansion coefficient with temperatures at different pressures. Thermal expansion is critical to investigate the thermodynamic and thermoelastic behavior of the solids at different temperatures. From Fig. 4, it is observed that the thermal expansion α grows exponentially up to room temperature. Above 300 K, the growth becomes slow and gradually approaches a linear increase. The upward trend

is less pronounced at high temperatures. The thermal expansion coefficient decreases significantly further increase of pressure at varying temperatures, as depicted in Fig. 4. At 300 K and zero pressure (see Table 2), the obtained values of the thermal expansion coefficient α for Sr_2RuO_4 and $\text{Sr}_2\text{RuO}_2\text{F}_2$ compounds are $4.58 \times 10^{-5} \text{ K}^{-1}$ and $4.62 \times 10^{-5} \text{ K}^{-1}$, respectively. The superconductor Sr_2RuO_4 has a lower thermal expansion coefficient than the $\text{Sr}_2\text{RuO}_2\text{F}_2$ alloy. Usually, it is attributed to the high melting point of Sr_2RuO_4 [29].

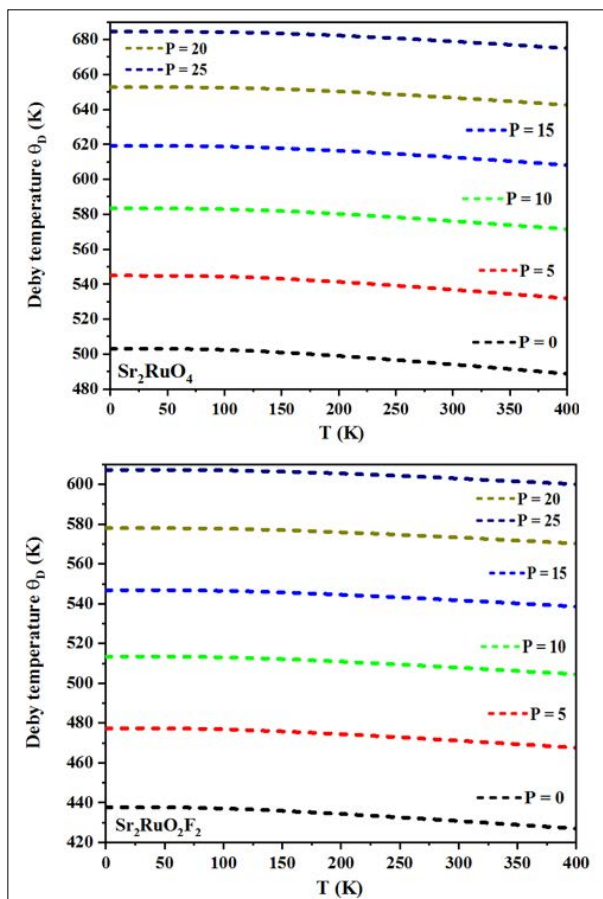


Figure 5: The Debye temperature as a function of temperature at different pressures.

The Debye temperature θ_D is an extremely significant feature of materials that can be employed to determine the thermal properties of solids. As the temperature rises beyond absolute zero, the atoms of the crystal solid gradually vibrate to Debye's temperature. θ_D represents the temperature at which the vibrations reach their maximum possible modes, and it is a reasonable estimate of the hardness of solids [30]. Fig. 5. exhibits the Debye temperature as a function of different temperatures, respectively, for the Sr_2RuO_4 ternary alloy and the $\text{Sr}_2\text{RuO}_2\text{F}_2$ quaternary alloy at various pressures. At a particular pressure, Debye temperature θ_D is almost constant from 0 K to 100 K, meaning that the crystals have a weak anharmonicity and slightly expand in this temperature range. When $T > 100$ K, θ_D decreases linearly with rising temperature,

reflecting the change in the vibrational spectra of atoms with temperature. At room temperature and zero pressure, the values of θ_D are 494.09 K and 430.67 K for Sr_2RuO_4 and $\text{Sr}_2\text{RuO}_2\text{F}_2$, respectively.

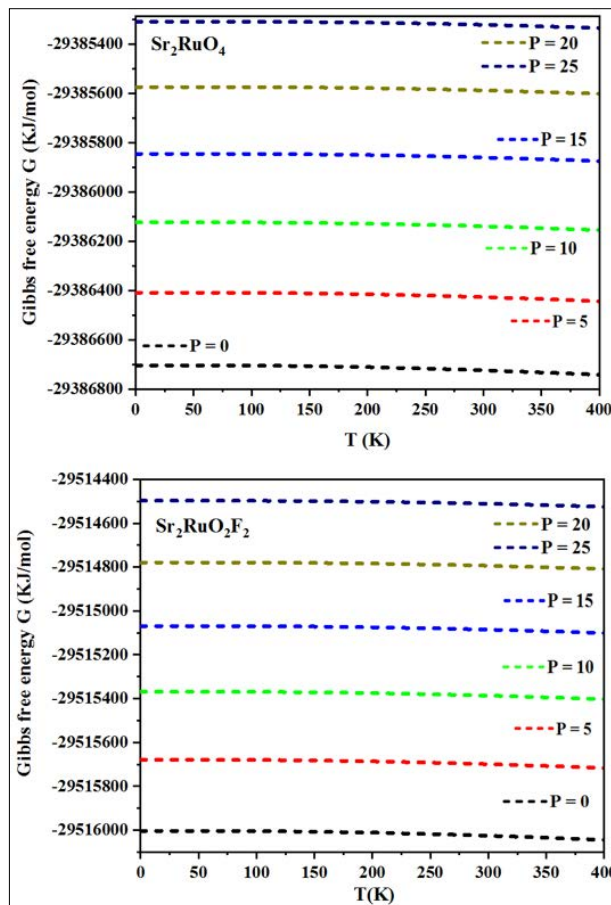


Figure 6: Gibbs free energy (G) as a function of temperature at different pressures

The temperature and pressure dependence of the Gibbs free energy (G) is shown in Fig. 6. At a fixed temperature, the Gibbs free energy values grow intensively as the pressure increases. On the other hand, G slightly diminishes with increasing temperature at a given pressure.

The Grüneisen parameter (γ) estimates the alteration in the frequency of the crystal lattice vibration and describes the influence of temperature or pressure on lattice volume and phonon frequencies [31]. The Grüneisen parameter γ for both materials at $P = 0$ GPa is approximately constant when $T < 50$ K, and monotonously decreases as the temperature increases up to 100 K. At a fixed temperature, the γ decreases dramatically with pressure, indicating that the temperature has a minor effect on the Grüneisen character (see Fig. 7).

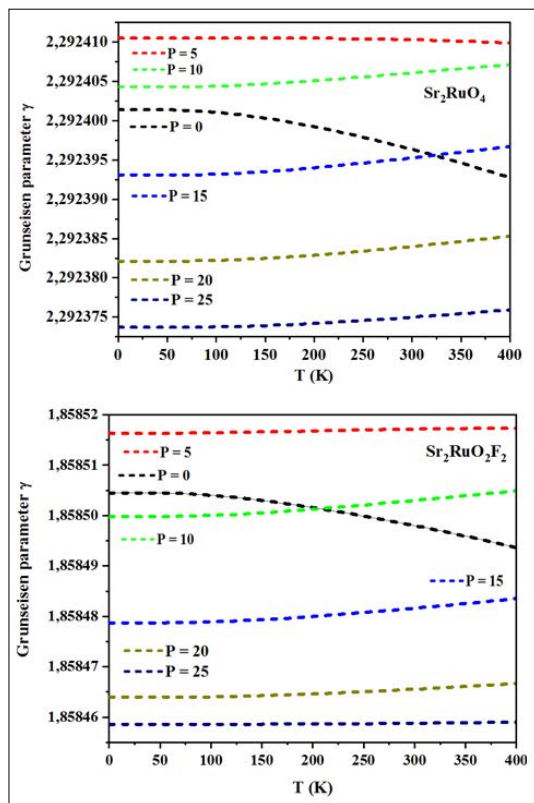


Figure 7: The Grüneisen parameter γ as a function of temperature at different pressures

In general terms, the heat capacity of a substance is a significant feature that provides the necessary comprehension and relevant analysis of vibrational characteristics. The temperature dependence of heat capacity at constant volume C_v and constant pressure C_p for Sr_2RuO_4 and $\text{Sr}_2\text{RuO}_2\text{F}_2$ compounds are plotted in Fig. 8. Both C_v and C_p obey T³ at low-temperature and abruptly jump with the temperature at a given pressure. The specific heat capacities present a robust dependence on temperature due to the Debye model based on the anharmonic approximation and are weakly sensitive to the pressure variation. At higher temperatures, the C_v and C_p parameters approach the Dulong-Petit limit [29].

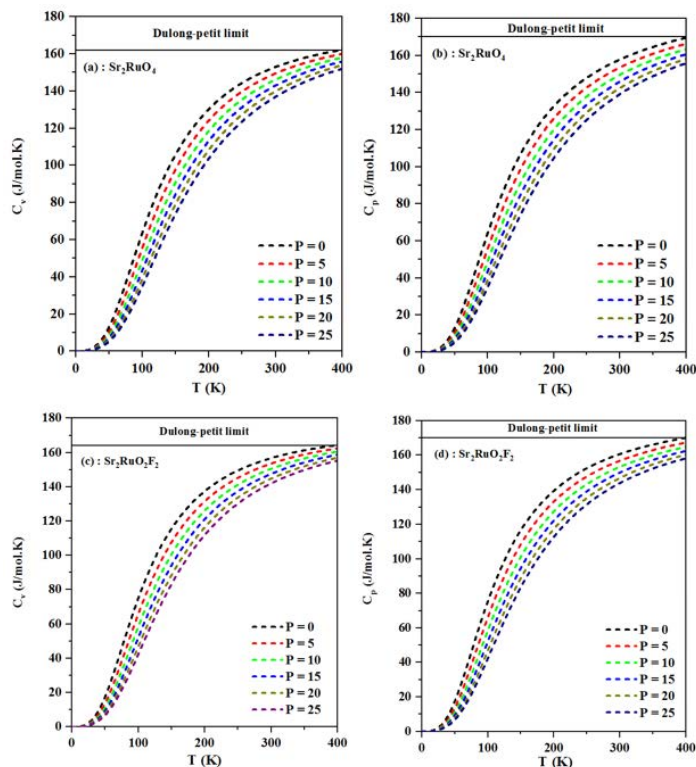


Figure 8: The heat capacity as a function of temperature at different pressures

Table 2: The calculated elastic parameters shear (G) and bulk (B) moduli, Poisson's ratio (ν), Young's modulus (E), Cauchy relation (C_v) using the Voigt, Reuss and Hill approximations

Parameters	Sr2RuO4	Sr2RuO2F2
Voigt bulk modulus B _v (GPa)	317.20	409.38
Voigt shear modulus G _v (GPa)	102.09	143.36
Reuss bulk modulus B _r (GPa)	317.08	368.88
Reuss shear modulus G _r (GPa)	85.11	32.49
Hill bulk modulus B _h (GPa)	317.14	389.13
Hill shear modulus G _h (GPa)	93.60	87.92
B _h /G _h	3.38	4.42
Voigt Young modulus E	276.60	385.12
Voigt Poisson ratio ν	0.35	0.34
Reuss Young modulus E	234.36	94.68
Reuss Poisson ratio ν	0.38	0.46
Hill Young modulus E	255.65	245.30
Hill Poisson ratio ν	0.37	0.39
Λ	0.10	0.63
C _v (GPa)	234.5	506.2

Conclusion

In summary, the first-principles calculations based on the DFT theory have been employed, using the FP-LAPW method, to investigate the elastic and thermodynamic properties of Sr₂RuO₄ and Sr₂RuO₂F₂. It is found that elastic constants of the studied compounds satisfy all of the mechanical stability criteria, indicating their structural stability. The temperature and pressure-dependent thermal properties were investigated using the quasi-harmonic approximation, providing a good description of free Gibbs energy G, Debye temperature θ_D, and heat capacity C_v in the pressure range from 0 to 25 GPa and temperature range from 0 to 400 K.

Acknowledgments

The authors are grateful to Prof. P. Blaha and Prof. K. Schwarz at the Vienna Technical University for the Wien2k package and the group of WIEN2K for useful discussions.

References

- OWENS Frank J, POOLE Charles P (2002) the new superconductors. Springer US.
- BRAICOVICH Lucio, AMENT LJP, BISOGNI Valentina, F Forte, C Aruta, et al. (2009) Dispersion of magnetic excitations in the cuprate La₂CuO₄ and CaCuO₂ compounds measured using resonant x-ray scattering. Physical review letters 102: 167401.
- HUANG Q, SOUBEYROUX JL, CHMAISSEM O, I Natali Sora, A Santoro, et al. (1994) Neutron powder diffraction study of the crystal structures of Sr₂RuO₄ and Sr₂IrO₄ at room temperature and at 10 K. Journal of Solid State Chemistry 112: 355-361.
- MAENO Yoshiteru, YOSHIDA Koji, HASHIMOTO Hiroaki, Shuji Nishizaki, Shin-ichi Ikeda, et al. (1997) Two-dimensional Fermi liquid behavior of the superconductor Sr₂RuO₄. Journal of the Physical Society of Japan 66: 1405-1408.
- YOKOYA Takayoshi, CHAINANIA, TAKAHASHI T (1996) Evidence for correlation effects in Sr₂ RuO₄ from resonant and x-ray photoemission spectroscopy. Physical Review B 53: 8151.
- M Braden, Y Sidis, P Bourges, P Pfeuty, J Kulda, Z Mao, et al. (2002) Inelastic neutron scattering study of magnetic excitations in Sr₂RuO₄. Physical Review B 66: 064522.
- Katsufuji T, Kasai M, Tokura Y (1996) In-Plane and Out-of-Plane Optical Spectra of Sr₂RuO₄. Physical Review Letters 76: 126-129.
- Maeno Y, Ando T, Mori Y, Ohmichi E, Ikeda S, et al. (1998) Enhancement of Superconductivity of Sr₂RuO₄ to 3K by Embedded Metallic Microdomains. Physical Review Letters 81: 3765-3768.
- EZ Kurmaev, S Stadler, DL Ederer, Y Harada, S Shin, et al. (1998) Electronic structure of Sr₂RuO₄: X-ray fluorescence emission study. Physical Review B 57: 1558-1562.
- Shen KM, Shen Z.-X (2007) Doping Evolution of the Cuprate Superconductors from High-Resolution ARPES. Lecture Notes in Physics 715: 243-270. Springer, Berlin, Heidelberg.
- MAENO Yoshiteru, YOSHIDA Koji, HASHIMOTO Hiroaki, Shuji Nishizaki, Shin-ichi Ikeda, et al. (1997) Two-Dimensional Fermi Liquid Behavior of the Superconductor Sr₂RuO₄. Journal of the Physical Society of Japan 66: 1405-1408.
- Maeno Y, Hashimoto H, Yoshida K, Nishizaki S, Fujita T, et al. (1994) Superconductivity in a layered perovskite without copper. Nature 372: 532.
- OGUCHI Tamio (1995) Electronic band structure of the superconductor Sr₂RuO₄. Physical Review B 51: 1385.
- BLAHA Peter, SCHWARZ Karlheinz, SORANTIN P (1990) Full-potential, linearized augmented plane wave programs for crystalline systems. Computer physics communications 59: 399-415.
- PERDEW John P, BURKE Kieron, ERNZERHOF Matthias (1996) Generalized gradient approximation made simple. Physical review letters 77: 3865.
- TRAN Fabien, BLAHA Peter (2009) Accurate band gaps of semiconductors and insulators with a semilocal exchange-correlation potential. Physical review letters 102: 226401.
- ZIATI Meryem, EZ-ZAHRAOUY Hamid (2021) Effect of uniaxial strain on structural, electronic and optical properties of Sr₂RuO₄-xFx: A DFT study. Chemical Physics 544 : 111132.
- MARTÍNEZ JL, PRIETO C, RODRÍGUEZ-CARVAJAL J,

- et al. Structural and magnetic properties of Sr_2RuO_4 -type oxides. *Journal of magnetism and magnetic materials* 140: 179-180.
19. SHANG SL, KIM DE, ZACHERL CL (2012) Effects of alloying elements and temperature on the elastic properties of dilute Ni-base superalloys from first-principles calculations. *Journal of Applied Physics* 112: 053515.
 20. HILL Richard (1952) the elastic behaviour of a crystalline aggregate. *Proceedings of the Physical Society. Section A* 65: 349.
 21. DONG Huafeng, CHEN Changqing, WANG Shanying, Wenhui Duan, Jingbo Li, et al. (2013) Elastic properties of tetragonal BiFeO_3 from first-principles calculations. *Applied Physics Letters* 102: 182905.
 22. PUGH SF (1954) XCII. Relations between the elastic moduli and the plastic properties of polycrystalline pure metals. *The London, Edinburgh, and Dublin Philosophical Magazine and Journal of Science* 45: 823-843.
 23. WU Zhi-jian, ZHAO Er-jun, XIANG Hong-ping, Xian-feng Hao, Xiao-juan Liu, et al. (2007) Crystal structures and elastic properties of superhard IrN_2 and IrN_3 from first principles. *Physical Review B* 76: 054115.
 24. CHIROMAWA, Idris Muhammad, SHAARI, Amiruddin, RAZALI, Razif, et al. (2021) First-principles investigation of structural, elastic, electronic and thermodynamic properties of strongly correlated ternary system: The DFT+ U approach. *Materials Science in Semiconductor Processing* 127: 105741.
 25. NIELSEN OH, MARTIN Richard M (1983) First-principles calculation of stress. *Physical Review Letters* 50: 697.
 26. NIELSEN OH, MARTIN Richard M (1985) Quantum-mechanical theory of stress and force. *Physical Review B* 32: 3780.
 27. GHOSH G (2015) A first-principles study of cementite (Fe_3C) and its alloyed counterparts: Elastic constants, elastic anisotropies, and isotropic elastic moduli. *AIP Advances* 5: 087102.
 28. HAO, Xi-Ping, CUI, Hong-Ling, LV, Zhen-Lon g, et al. Electronic and elastic properties of Sr_2RuO_4 with pressure effects by first principles calculation. *Physica B: Condensed Matter* 441: 62-67.
 29. MAO, Z. Q., MAENOAB, Y., et FUKAZAWA, H. Crystal growth of Sr_2RuO_4 . *Materials research bulletin* 35: 1813-1824.
 30. ZHANG Ji-Dong, CHENG Xin-Lu, LI De-Hua (2011) First-principles study of the elastic and thermodynamic properties of HfB_2 with AlB_2 structure under high pressure. *Journal of alloys and compounds* 509: 9577-9582.
 31. Fu H, Liu W, Gao T (2011) Structural, elastic and thermodynamic properties of Ti_2SC . *Bull Mater Sci* 34: 1617-1625.